

DreamPartGen: Semantically Grounded Part-Level 3D Generation via Collaborative Latent Denoising

Tianjiao Yu, Xinzhuo Li, Muntasir Wahed, Jerry Xiong, Yifan Shen, Ying Shen, Ismini Lourentzou

{ty41, lourent2}@illinois.edu

University of Illinois Urbana - Champaign

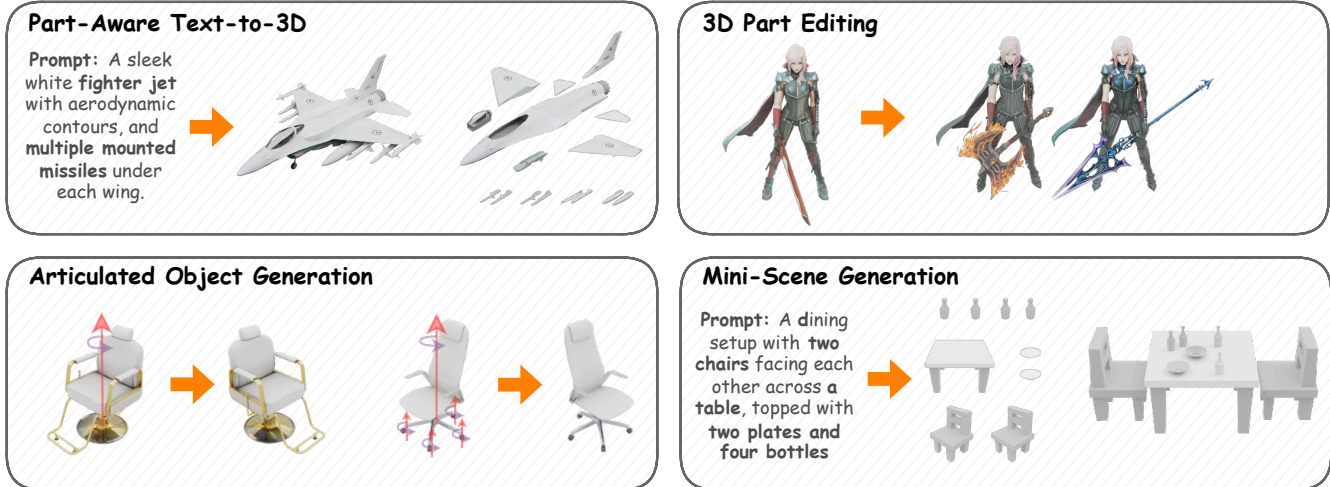


Figure 1: DreamPartGen connects part-level geometry and appearance with language-driven relational semantics, providing precise control over how parts are modified, arranged, and contextualized. This unified representation enables a wide range of downstream applications, including fine-grained part editing, articulated object generation, and mini-scene synthesis.

Abstract. Understanding and generating 3D objects as compositions of meaningful parts is fundamental to human perception and reasoning. However, most text-to-3D methods overlook the semantic and functional structure of parts. While recent part-aware approaches introduce decomposition, they remain largely geometry-focused, lacking semantic grounding and failing to model how parts align with textual descriptions or their inter-part relations. We propose **DreamPartGen**, a framework for semantically grounded, part-aware text-to-3D generation. DreamPartGen introduces Duplex Part Latents (DPLs) that jointly model each part’s geometry and appearance, and Relational Semantic Latents (RSLs) that capture inter-part dependencies derived from language. A synchronized co-denoising process enforces mutual geometric and semantic consistency, enabling coherent, interpretable, and text-aligned 3D synthesis. Across multiple benchmarks, **DreamPartGen** delivers state-of-the-art performance in geometric fidelity ($\downarrow 53\%$ Chamfer Distance) and text–shape alignment ($\geq \uparrow 20\%$ CLIP/ULIP), while producing compositionally consistent and controllable parts.

<https://plan-lab.github.io/dreampartgen>



1. Introduction

Many text prompts for 3D generation specify not only *what* parts an object has, but *how* they relate (e.g., a handle *attached to* a mug, wheels *symmetric on* a chassis, a lid *on top of* a box). Capturing these part-level relations is crucial for controllable generation

and downstream use cases such as part editing and articulated synthesis [17, 30, 53]. However, most text-to-3D methods operate on monolithic latents that entangle geometry, appearance, and semantics, with no explicit representation of part identities or inter-part relations [6, 21, 22, 25, 33, 39, 44]. Recent part-aware methods take a step forward by synthe-

sizing objects from part primitives guided by part segmentations or bounding boxes [5, 11, 16, 24, 48]. Although these approaches improve geometric granularity, they are still brittle to segmentation noise and can be difficult to scale across diverse categories and prompts. More importantly, many part-based frameworks still treat parts as geometrically isolated units. They do not model inter-part relations as explicit variables, and language remains largely non-operational.

Part-aware text-to-3D generation requires a semantically grounded representation in which parts are meaningful entities, and language provides relational structure in addition to describing appearance. Concretely, we introduce **DreamPartGen**, a language-grounded, collaborative part-latent diffusion framework that treats compositional semantics as an explicit representation during denoising. Each object is encoded into **Duplex Part Latents (DPLs)**, paired 3D and 2D latent sequences that jointly capture a part’s geometry and appearance, whereas a learnable identifier embedding preserves slot identity across timesteps and instances, keeping parts trackable throughout diffusion. In parallel, we introduce **Relational Semantic Latents (RSLs)**, compact text-derived latents that encode part-level attributes and inter-part relations. Rather than using language only as one-shot conditioning, DreamPartGen performs synchronized co-denoising: DPLs and RSLs co-evolve through part-level and object-level synchronization so that geometry and appearance are refined under persistent, language-derived relational guidance, enforcing mutual geometric–semantic consistency.

To enable supervision at scale, we curate **PartRel3D**, a large-scale relational dataset that augments each object with canonicalized functional and spatial triplets linking parts through explicit semantic predicates. These canonicalized relations are encoded into RSLs, allowing the model to learn assembly-level consistency directly from language. Trained on PartRel3D, DreamPartGen surpasses prior text-to-3D and part-aware baselines, achieving substantial improvements in geometric fidelity ($\downarrow 53\%$ CD, $\downarrow 33\%$ EMD) and text–shape alignment ($\geq 20\%$ \uparrow CLIP/ULIP). We also evaluate generalization to rare parts and held-out relation predicates, improving over prior part-based baselines ($14.7\text{--}16.3\%$ \downarrow

Render-FID, $68.2\text{--}71.2\%$ \downarrow CD, $39.6\text{--}47.9\%$ \uparrow ULIP-T). In summary, our contributions are:

- We introduce **DreamPartGen**, a language-grounded collaborative diffusion framework that unifies geometric, visual, and relational reasoning for coherent and interpretable part-level text-to-3D synthesis.
- We introduce **DPLs** and **RSLs** as complementary representations that jointly encode part geometry, appearance, and inter-part relations and are refined together via synchronized co-denoising.
- We curate **PartRel3D**, a large-scale relational dataset with 300K functional and spatial triplets for explicit language-based supervision of inter-part relations across 175 object categories.
- Across benchmarks, **DreamPartGen** achieves substantial gains in fidelity, language alignment, and controllable part-aware generation.

2. Related Work

Text-to-3D Generation. Early text-to-3D approaches such as DreamFusion [33], ProlificDreamer [44], and LucidDreamer [21] leverage the idea of score distillation sampling (SDS) to generate 3D assets from 2D diffusion priors. While effective for producing single objects, SDS approaches often suffer from low fidelity and poor multi-view consistency [6, 13, 19, 22, 35, 39]. Recent works improve training stability and geometric realism by incorporating differentiable rendering with explicit 3D representations, including Gaussian splatting in DreamGaussian [40] and GaussianDreamer [50], voxel- or mesh-based parameterizations in Clay [55], and hybrid autoregressive architectures such as Trellis [29, 45, 51]. These advances establish strong foundations for high-quality 3D generation, but typically focus on whole objects, without modeling explicit part structure or relational semantics.

Part-level 3D Generation. To address the limitations of object generation, several methods introduce part-aware modeling [12, 18, 23, 48, 49]. Part123 [24] and Salad [16] focus on part segmentation and assembly, while PartGen [5] leverages part decomposition for generative modeling. CoPart [10] ex-

tends diffusion models with dual priors over part-level 2D and 3D latents, enabling cross-modality and cross-part mutual guidance. Additionally, works such as PartGS [11] and Part²GS [53] adapt Gaussian splatting for articulated part-aware generation, demonstrating that part supervision yields controllable and physically plausible synthesis [26, 28, 38]. Despite these advances, prior approaches rely heavily on geometric signals such as bounding boxes [20, 32, 43, 57], leaving language guidance underexplored [2, 27, 37, 52, 56]. DreamPartGen introduces explicit relational semantic signals that persist throughout denoising, providing both fine-grained part refinement and relation-aware global planning cues directly from natural language.

3. DreamPartGen Method

While recent part-level formulations improve local shape and texture modeling [5, 7, 47], they primarily focus on representation quality and do not explicitly preserve *text-derived semantics* throughout denoising, which limits their text-to-3D capability and fine-grained controllability. Our key novelty is to introduce *persistent, language-derived relational semantic latents* that remain active throughout the denoising process, rather than using text only as a one-shot condition, and to synchronize them with part-level geometric latents.

To this end, we formulate part-based 3D generation as a semantically grounded collaborative diffusion process between two complementary latent representations: ① **Duplex Part Latents (DPLs)** (Sec. 3.1), which encode geometry and appearance of individual parts in a modular and disentangled manner, and ② **Relational Semantic Latents (RSLs)** (Sec. 3.2), a compact set of text-derived latent tokens that provide both local refinements and global planning signals. During denoising, DPLs and RSLs are synchronized through intra-part and inter-part attention (Sec. 3.3), enabling consistent part-level geometry-appearance alignment and language-guided part assembly.

3.1. Duplex Part Latents (DPLs)

The design of Duplex Part Latents (DPLs) is motivated by recent advances in structured latent representations for 3D generation, which demonstrate that compact latent sets can effectively encode both geometry and appearance [41, 45, 49]. However, existing unified latents primarily operate on voxel-aligned local features capturing shape and texture, but remain tied to spatial grids rather than semantic components. As a result, they lack modularity across objects and do not support explicit part-level disentanglement or relational reasoning. To address these limitations, we represent each object as a collection of N semantic parts $O = \{p_i\}_{i=1}^N$, and encode each part using three complementary elements:

- **3D tokens:** For each part mesh p_i , we sample surface points with associated normals and pass them through a 3D VAE encoder [15, 54], producing a latent sequence $\mathbf{L}_i^{3D} \in \mathbb{R}^{T_{3D} \times d}$, where T_{3D} denotes the number of 3D latent tokens and d their embedding dimension, capturing local geometry and spatial structure.
- **2D tokens:** Each part is also rendered from multiple viewpoints, and the resulting images are passed through a pretrained image VAE [4], yielding $\mathbf{L}_i^{2D} \in \mathbb{R}^{T_{2D} \times d}$, which encodes color, texture, and shading cues.
- **Part-identity:** To stabilize part tracking across denoising steps, we assign a learnable identifier embedding $e_i \in \mathbb{R}^d$ to each part. These identifiers act as persistent slot identities, binding each latent to its corresponding part and preventing slot swapping across denoising, while relational reasoning layers flexibly reorganize cross-part interactions.

Compared to prior structured latent designs [23, 45], Duplex Part Latents (DPLs) are designed to preserve semantic independence while enabling language-conditioned relational reasoning. This yields several key benefits. First, the architecture is permutation-robust to the input ordering of parts, as the learnable part-identity embeddings prevent semantics from depending on the input part order. Second, the identifiers provide *slot persistence* across denoising timesteps, improving stability of intra-part and inter-part synchronization. Third, because each

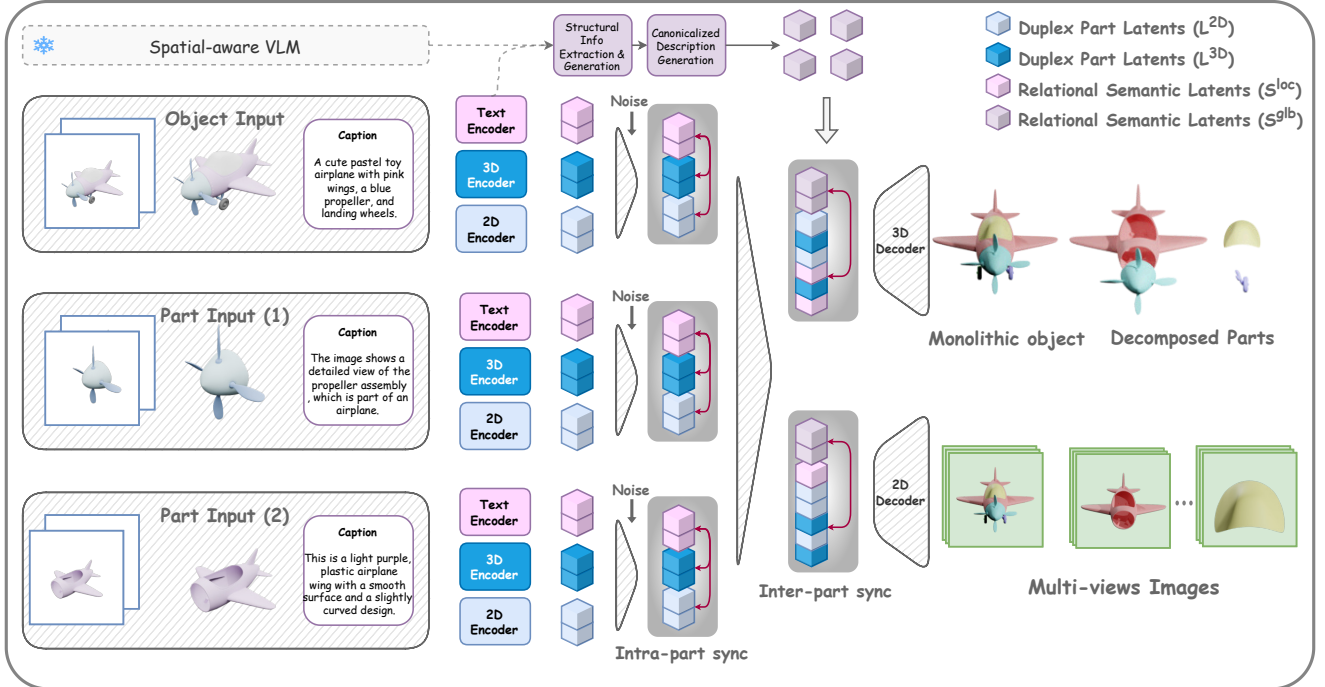


Figure 2: DreamPartGen Overview. DreamPartGen performs text-guided 3D generation by jointly denoising geometry, appearance, and relational semantics. Each object is decomposed into parts represented as **Duplex Part Latents (DPLs)** from 3D and 2D encoders, while **Relational Semantic Latents (RSLs)** encode text-derived details and global structure. Through intra-part (geometry–appearance alignment) and inter-part (relational planning via language) synchronization, DreamPartGen co-denoises DPLs and RSLs, enabling semantically grounded reconstruction of coherent part-aware 3D objects.

part is represented as its own modular latent triplet $(\mathbf{L}_i^{3D}, \mathbf{L}_i^{2D}, e_i)$, DPLs naturally support cross-object generalization, enabling latent transfer between objects with shared functional components. Finally, DPLs are lightweight and modular, making them directly suitable for integration with diffusion and facilitating coherent multi-part synthesis and reasoning.

3.2. Relational Semantic Latents (RSLs).

While DPLs provide modular and disentangled representations for individual parts, they do not by themselves guarantee that the assembled object is globally coherent. This reflects a broader challenge in part-based 3D generation: local geometry and appearance can be faithfully synthesized, yet without explicit semantic coordination, the resulting object structure may violate plausible spatial or functional relations [6, 22, 44]. To address this gap, we introduce Relational Semantic Latents (RSLs), a compact set of

language-derived latent tokens that provide semantic control signals for part interactions through two roles: persistent global planners and diffused local refiners. In particular, global relational tokens \mathbf{S}^{glb} persist as fixed structural conditions, while local semantic tokens \mathbf{S}^{loc} are diffused and denoised alongside the part latents to refine part-level details.

Global Relational Tokens. At the object level, we extract relational phrases from whole-object and part-level descriptions (e.g., “the seat is above the legs,” “the propeller is attached to the fuselage,” “the two wings are symmetric”, etc.). Each phrase is canonicalized into a triplet (i, j, ρ) , where i and j denote parts and ρ is a relation predicate such as support, attach, symmetry, or articulation. These triplets are assembled into a relational graph and projected into the latent space (Figure 3) to yield a set of global relational tokens:

$$\mathbf{S}^{\text{glb}} = \{\mathbf{s}_{ij,\rho}^{\text{glb}}\}_{(i,j,\rho) \in \mathcal{R}}, \quad \mathbf{s}_{ij,\rho}^{\text{glb}} \in \mathbb{R}^d. \quad (1)$$

In this way, \mathbf{S}^{glb} constitutes a relational graph latent, where each token encodes how two parts are semantically related. These tokens persist throughout the diffusion process and are injected into object-level synchronization, functioning both as semantic planners that specify inter-part relations and as structural conditions that enforce coherent assembly. Unlike prior geometry-based approaches, they are derived entirely from natural language, embedding functional and structural priors without explicit geometric supervision.

Local Semantic Tokens. At the part level, we encode fine-grained semantic cues (e.g., “metallic blade,” “wooden handle”, etc.) to refine material and appearance. Each phrase is encoded and projected into the latent space to yield K_m local semantic tokens:

$$\mathbf{S}^{\text{loc}} = \{\mathbf{s}_m^{\text{loc}}\}_{m=1}^{K_m}, \quad \mathbf{s}_m^{\text{loc}} \in \mathbb{R}^d, \quad (2)$$

which directly interact with the structural DPL tokens to enhance geometric fidelity and appearance under semantic constraints. Compared to geometry-only latents, RSLs are compact, interpretable, and flexible: their number adapts to object complexity, and additional tokens can be easily obtained by generating short textual descriptions for new parts or relations. Unlike one-shot text conditioning [22, 33], we inject these tokens at every denoising step, enabling iterative semantic refinement. During diffusion, we apply the standard forward noising process to obtain $\mathbf{S}^{\text{loc},t}$ from the clean tokens \mathbf{S}^{loc} . The noised local semantic tokens $\mathbf{S}^{\text{loc},t}$ are injected at each step t to synchronize with the noised part latents and refine part-specific appearance.

3.3. Semantically-Grounded Part Generation

We first instantiate DPLs by encoding each part mesh p_i into geometry and appearance token sequences ($\mathbf{L}_i^{3D}, \mathbf{L}_i^{2D}$) using the 3D VAE encoder and the pre-trained image VAE encoder introduced in §3.1, and tag each part with a learnable identifier e_i . We instantiate RSLs by encoding extracted relational/attribute phrases with a frozen text encoder $\mathcal{E}_{\text{text}}$ [42] followed by a learned projection ϕ_{text} , yielding $(\mathbf{S}^{\text{glb}}, \mathbf{S}^{\text{loc}})$. To enable coherent generation, DPLs and RSLs interact throughout denoising via a two-level synchroniza-

tion mechanism. Specifically, we perform diffusion over the noised part latents $\{\mathbf{L}_i^{3D,t}, \mathbf{L}_i^{2D,t}\}_{i=1}^N$ and the noised local semantic tokens $\mathbf{S}^{\text{loc},t}$, while keeping the global relational tokens \mathbf{S}^{glb} persistent as fixed structural conditions. At each step t , we apply *intra-part synchronization* to align geometry and appearance within each part under local semantic guidance, and then *inter-part synchronization* to propagate context across parts and enforce global relational constraints.

Intra-Part Synchronization. At diffusion step t , each part p_i is represented by a noised geometry latent sequence $\mathbf{L}_i^{3D,t}$ and a noised appearance latent sequence $\mathbf{L}_i^{2D,t}$. We first synchronize these two streams to maintain intra-part geometry-appearance consistency, and then inject noised local semantic tokens $\mathbf{S}^{\text{loc},t}$ to refine part-specific geometric and visual details according to semantic cues. Formally,

$$\begin{aligned} \mathbf{L}_i^{3D,t} &\leftarrow \mathbf{L}_i^{3D,t} + \alpha_{3D} \cdot \text{Attn}(\mathbf{L}_i^{3D,t}, \mathbf{L}_i^{2D,t}), \\ \mathbf{L}_i^{2D,t} &\leftarrow \mathbf{L}_i^{2D,t} + \alpha_{2D} \cdot \text{Attn}(\mathbf{L}_i^{2D,t}, \mathbf{L}_i^{3D,t}), \\ \mathbf{L}_i^{3D,t} &\leftarrow \mathbf{L}_i^{3D,t} + \lambda_{3D} \cdot \text{Attn}(\mathbf{L}_i^{3D,t}, \mathbf{S}^{\text{loc},t}), \\ \mathbf{L}_i^{2D,t} &\leftarrow \mathbf{L}_i^{2D,t} + \lambda_{2D} \cdot \text{Attn}(\mathbf{L}_i^{2D,t}, \mathbf{S}^{\text{loc},t}), \end{aligned} \quad (3)$$

where $\alpha_{3D}, \alpha_{2D}, \lambda_{3D}, \lambda_{2D}$ are fusion coefficients.

Inter-Part Synchronization. After intra-part alignment, we propagate context across parts to encourage globally consistent assembly in two complementary ways: (i) direct message passing among all part latents to share global context, and (ii) relational guidance from persistent global tokens \mathbf{S}^{glb} that encode inter-part predicates (e.g., support, attach, symmetry, articulation). Finally, we update \mathbf{S}^{glb} via bottom-up grounding from the current part latents, refining the relational plan based on synthesized geometric and appearance evidence. Concretely,

$$\begin{aligned} \mathbf{L}_i^{3D,t} &\leftarrow \mathbf{L}_i^{3D,t} + \text{Attn}(\mathbf{L}_i^{3D,t}, \{\mathbf{L}_j^{3D,t}\}_{j=1}^N), \\ \mathbf{L}_i^{2D,t} &\leftarrow \mathbf{L}_i^{2D,t} + \text{Attn}(\mathbf{L}_i^{2D,t}, \{\mathbf{L}_j^{2D,t}\}_{j=1}^N), \\ \mathbf{L}_i^{3D,t} &\leftarrow \mathbf{L}_i^{3D,t} + \beta_{3D} \cdot \text{Attn}(\mathbf{L}_i^{3D,t}, \mathbf{S}^{\text{glb}}), \\ \mathbf{L}_i^{2D,t} &\leftarrow \mathbf{L}_i^{2D,t} + \beta_{2D} \cdot \text{Attn}(\mathbf{L}_i^{2D,t}, \mathbf{S}^{\text{glb}}), \\ \mathbf{S}^{\text{glb}} &\leftarrow \mathbf{S}^{\text{glb}} + \eta \cdot \text{Attn}(\mathbf{S}^{\text{glb}}, \{\text{Pool}(\mathbf{L}_i^{3D,t}, \mathbf{L}_i^{2D,t})\}_{i=1}^N). \end{aligned} \quad (4)$$

where $\text{Pool}(\cdot)$ aggregates each part’s latent se-

quences into a compact summary for bottom-up grounding. Here, \mathbf{S}^{glb} is updated deterministically as a planner state that remains available as a fixed relational condition at every timestep.

Optimization. Training proceeds in two phases. In the first phase, we optimize diffusion objectives for both 3D and 2D DPLs under semantic conditioning from RSLs. For timesteps $t \sim \mathcal{U}\{1, \dots, T\}$ and noise $\varepsilon \sim \mathcal{N}(0, I)$, the per-part diffusion losses are:

$$\begin{aligned} \mathcal{L}_{\text{diff}}^{3\text{D}} &= \frac{1}{N} \sum_{i=1}^N \mathbb{E}_{t,\varepsilon} \left[\left\| \varepsilon - \mathcal{N}_{3\text{D}}(\mathbf{L}_i^{3\text{D},t}, \mathbf{L}_i^{2\text{D},t}, \mathbf{S}^{\text{glb}}, \mathbf{S}^{\text{loc},t}, t) \right\|_2^2 \right], \\ \mathcal{L}_{\text{diff}}^{2\text{D}} &= \frac{1}{N} \sum_{i=1}^N \mathbb{E}_{t,\varepsilon} \left[\left\| \varepsilon - \mathcal{N}_{2\text{D}}(\mathbf{L}_i^{2\text{D},t}, \mathbf{L}_i^{3\text{D},t}, \mathbf{S}^{\text{glb}}, \mathbf{S}^{\text{loc},t}, t) \right\|_2^2 \right]. \end{aligned} \quad (5)$$

In the second phase, we fine-tune the model jointly across the 3D and 2D part denoisers and synchronization modules, using an SNR-based curriculum that progressively shifts focus from faithful denoising toward relational alignment. The overall objective combines all components:

$$\mathcal{L} = \mathbb{E}_t \left[w_{\text{syn}}(t) (\mathcal{L}_{\text{diff}}^{3\text{D}} + \mathcal{L}_{\text{diff}}^{2\text{D}}) \right], \quad (6)$$

where weights follow an SNR-based schedule $w_{\text{syn}}(t) = \frac{\text{SNR}(t)}{1+\text{SNR}(t)}$, with $\text{SNR}(t) = \alpha_t^2 / \sigma_t^2$ defined by the diffusion coefficients.

Inference. At test time, we encode the input prompt into local semantic tokens \mathbf{S}^{loc} and global planner tokens \mathbf{S}^{glb} . When explicit triplets are available (e.g., provided by the user or an external parser), they are encoded as \mathbf{S}^{glb} ; otherwise, we default to prompt-only conditioning instead of relying on external VLMs to supplement the triplets. We then initialize part latents by sampling Gaussian noise for the geometry and appearance streams, $\{\mathbf{L}_i^{3\text{D},T}, \mathbf{L}_i^{2\text{D},T}\}_{i=1}^N$, and initialize the local semantic stream by applying the same forward noising process used in training to obtain $\mathbf{S}^{\text{loc},T}$ from \mathbf{S}^{loc} . From timestep T to 1, we jointly denoise $\{\mathbf{L}_i^{3\text{D},t}, \mathbf{L}_i^{2\text{D},t}\}_{i=1}^N$ and $\mathbf{S}^{\text{loc},t}$ using the same part-level and object-level synchronization modules while conditioning on persistent \mathbf{S}^{glb} . After denoising, the final geometry latents $\{\mathbf{L}_i^{3\text{D},0}\}_{i=1}^N$ are decoded by the 3D VAE decoder to obtain part meshes, and the object is assembled from the decoded parts, with $\mathbf{L}_i^{2\text{D},0}$ used for appearance rendering when needed.

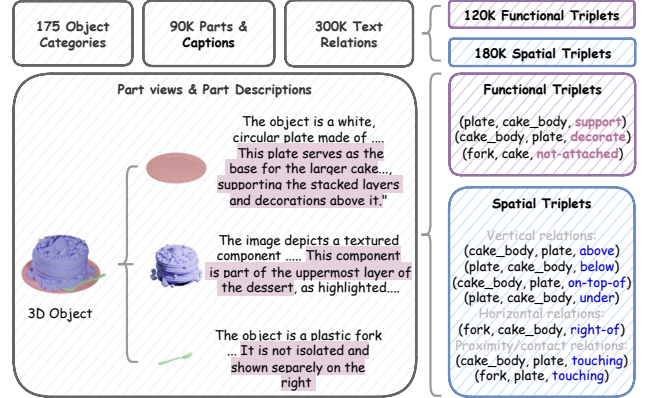


Figure 3: PartRel3D dataset overview of structured functional and spatial triplets for fine-grained inter-part semantic supervision.

4. PartRel3D Dataset

Existing 3D datasets such as PartNet [31], Objaverse [9], and PartVerse [10] provide large-scale geometric diversity but are limited in semantic grounding and relational coverage. They often include either geometry-only annotations or unconstrained text captions without consistent part correspondence, limiting their suitability for training models that understand object assembly (how parts connect) and semantics (what roles parts play). To overcome these limitations, we introduce **PartRel3D**, a large-scale, relationally annotated extension of PartVerse [10] that links part geometry, appearance, and language through explicit functional and spatial relationships. Each object in PartRel3D is augmented with canonicalized triplets that encode both functional dependencies (e.g., support, attach, hinge) and spatial arrangements (e.g., above, touching, aligned-with), providing large-scale supervision of assembly-level semantics in 3D (Figure 3).

Functional Triplets capture how parts interact in terms of support, attachment, and articulation. Given part- and object-level descriptions, we canonicalize phrases such as “legs support seat” or “handle attached to body” into triplets $(i, j, \rho^{\text{function}})$, where i, j are part indices and ρ^{function} is a functional predicate (e.g., support, attach, hinge, symmetry).

Spatial Triplets capture geometric and positional relations between parts. Each triplet has the same

Table 1: Quantitative evaluation on 3D object generation. Quantitative comparison with state-of-the-art methods on Objaverse, ShapeNet, ABO, and Partverse. Highlighted **best** and **second-best** results.

Method	Objaverse			ShapeNet			ABO			PartRel3D		
	CD↓	EMD↓	IoU↓									
Trellis	0.361	1.320	-	0.549	1.482	-	0.287	0.933	-	0.532	1.526	-
CLAY	0.318	1.245	-	0.527	1.503	-	0.321	1.022	-	0.410	1.646	-
HoloPart	0.334	1.298	0.494	0.478	1.354	0.542	0.269	0.911	0.529	0.355	1.623	0.716
PartCrafter	0.278	1.107	0.453	0.451	1.252	0.499	0.266	0.905	0.505	0.371	1.474	0.700
DreamPartGen	0.141	0.810	0.359	0.222	0.967	0.503	0.101	0.531	0.404	0.081	0.412	0.304

form $(i, j, \rho^{\text{spatial}})$, where i and j still index parts from the set of object parts \mathcal{P} , but ρ^{spatial} is a predicate drawn from a controlled vocabulary of interpretable, assembly-relevant predicates. These include vertical relations (above, below, on-top-of, under), horizontal relations (in-front-of, behind, left-of, right-of), containment relations (inside, surrounding), symmetry/arrangement (symmetric-with, parallel-to, aligned-with), proximity and contact relations (touching, attached-to, connected-with).

The resulting PartRel3D dataset contains approximately 11K part-labeled objects spanning 175 object categories, with over 90K individual parts and 300K canonicalized relational triplets. On average, each object contains 8.2 parts and 27 inter-part relations, providing dense structural supervision. Additional details, dataset statistics, and canonicalization criteria are available in the Appendix.

5. Experiments

Baselines. We compare against Trellis [45], CLAY [55], HoloPart [48], and PartCrafter [23], as they represent the current state of the art in 3D generation. These methods collectively capture the diversity of contemporary approaches from structured latent representations [45] to explicit part generation and assembly part-aware text-driven 3D [23]. Moreover, all of them provide open-source implementations, enabling fair and reproducible comparison under consistent training and evaluation protocols.

Metrics. Following prior work [55], we adopt both perceptual and structural metrics for text-to-3D eval-

uation. We report render-FID and render-KID computed from multi-view renderings to assess visual fidelity, and P-FID/P-KID computed in 3D feature space using PointNet++ [34]. Chamfer Distance (CD) and Earth Mover’s Distance (EMD) measure geometric precision.

For text–shape alignment, we compute similarity with CLIP-ViT/L-14 [36] and ULIP [46]. In particular, ULIP-T is defined as the inner product between normalized ULIP embeddings of the caption T and the generated shape S , $\text{ULIP-T}(T, S) = \langle E_T, E_S \rangle$, reflecting the semantic coherence between textual and geometric modalities.

We further use the average pairwise Intersection-over-Union (IoU) to evaluate the geometric independence of generated part meshes. Specifically, we voxelize each generated part in a shared canonical space using a $64 \times 64 \times 64$ grid, and compute the average pairwise IoU across all generated parts following [23]. Lower IoU indicates less inter-part overlap and therefore better part disentanglement. The ideal case is that generated parts are non-intersecting while remaining composable into a plausible object consistent with the ground-truth structure.

5.1. Quantitative Results

We evaluate geometric reconstruction quality across Objaverse [9], ShapeNet [3], ABO [8], and our PartRel3D. As shown in Table 1, DreamPartGen consistently achieves the lowest CD and EMD on all benchmarks, outperforming prior methods by large margins ($\downarrow 53\%$ CD and $\downarrow 33\%$ EMD on average). Moreover, DreamPartGen attains the lowest

Table 2: Text-shape alignment comparison. Quantitative comparison on Partverse. **Best** and **second-best** are highlighted.

Scope	Method	CLIP(N-T) \uparrow	CLIP(I-T) \uparrow	ULIP-T \uparrow
Object-level	Trellis	0.192	0.214	0.164
	CLAY	0.194	0.216	0.156
	HoloPart	0.186	0.206	0.155
	PartCrafter	0.187	0.207	0.162
	DreamPartGen	0.235	0.264	0.197
Part-level	Trellis	0.106	0.122	0.091
	CLAY	0.112	0.128	0.096
	HoloPart	0.130	0.141	0.113
	PartCrafter	0.125	0.145	0.109
	DreamPartGen	0.179	0.200	0.153

IoU scores (\downarrow 27.2% on average), reflecting stronger *geometry independence*, *i.e.*, the ability to generate non-intersecting yet composable parts that maintain object-level coherence.

We further assess text–shape alignment performance on the Partverse dataset following [10], where half of the test cases describe individual parts (*e.g.*, “a chair leg”), and the rest correspond to complete objects. As shown in Table 2, DreamPartGen improves text–shape alignment over the strongest baseline across all metrics by (\geq 20%) at the object level and (\geq 35%) at the part level, highlighting the effectiveness of RSLs for fine-grained semantic grounding.

5.2. Qualitative Results

Figure 4 highlights that, across diverse object categories, DreamPartGen consistently generates 3D objects with part-consistent and physically plausible assemblies. Compared to the strongest baselines, HoloPart [48] and PartCrafter [23], our method preserves fine-grained geometry more faithfully, maintains inter-part relationships better, and respects global structural constraints that are frequently violated by prior approaches. As illustrated, baselines frequently omit distorted parts or misplace them in space, for instance, generating wheels that float away from the chassis or misaligning small mechanical parts, leading to broken functional geometry in the first example. Similar failures appear in the second and third examples, where HoloPart produces a detached wing (airplane) or

Table 3: Ablation on Model Components. Quantitative evaluation on PartRel3D. **Best** and **second-best** are highlighted.

Method	CD \downarrow	EMD \downarrow	IoU \downarrow	ULIP-T \uparrow
HoloPart	1.482	0.226	0.318	0.112
PartCrafter	1.403	0.219	0.341	0.101
DreamPartGen	0.771	0.145	0.212	0.158
\times S^{glb}	2.892	0.292	0.587	0.084
\times S^{loc}	5.764	0.781	0.652	0.089
\times Part Identifier	1.709	0.277	0.438	0.091

head (humanoid), and both baselines exhibit surface tearing and holes around the neck, torso, and shoulders, indicating incomplete and unstable attachment geometry. DreamPartGen, by contrast, generates watertight meshes with intact intra-part connections, smoother surfaces, and correctly integrated parts. Finally, in the last row, baselines suffer from hollow torsos, shredded hand geometry, and broken limb attachments, while DreamPartGen maintains coherent small-part geometry and avoids the severe tearing and disintegration observed in prior methods. These results demonstrate that DreamPartGen’s relationally grounded generation maintains local part fidelity but also enforces globally consistent part connectivity even in complex articulated 3D structures.

5.3. Ablations

RSLs and Part Identity. Table 3 summarizes the contribution of each component in DreamPartGen, evaluated on a test subset of PartRel3D dataset and compared against strong part-aware baselines. We assess performance using geometric fidelity (CD, EMD), part-level separation via pairwise IoU, and text–shape alignment via ULIP-T, yielding a comprehensive view of both geometry and semantics. When removing the global relational tokens (\times S^{glb}), CD increases from 0.771 to 2.892 (\uparrow 275.1%), EMD increases from 0.145 to 0.292 (\uparrow 101.4%), and part overlap rises from IoU 0.212 to 0.587 (\uparrow 176.9%), while ULIP-T drops from 0.158 to 0.084 (\downarrow 46.8%), indicating that relational context is essential for preventing collisions and maintaining coherent assembly. Disabling local semantic tokens (\times S^{loc}) degrades

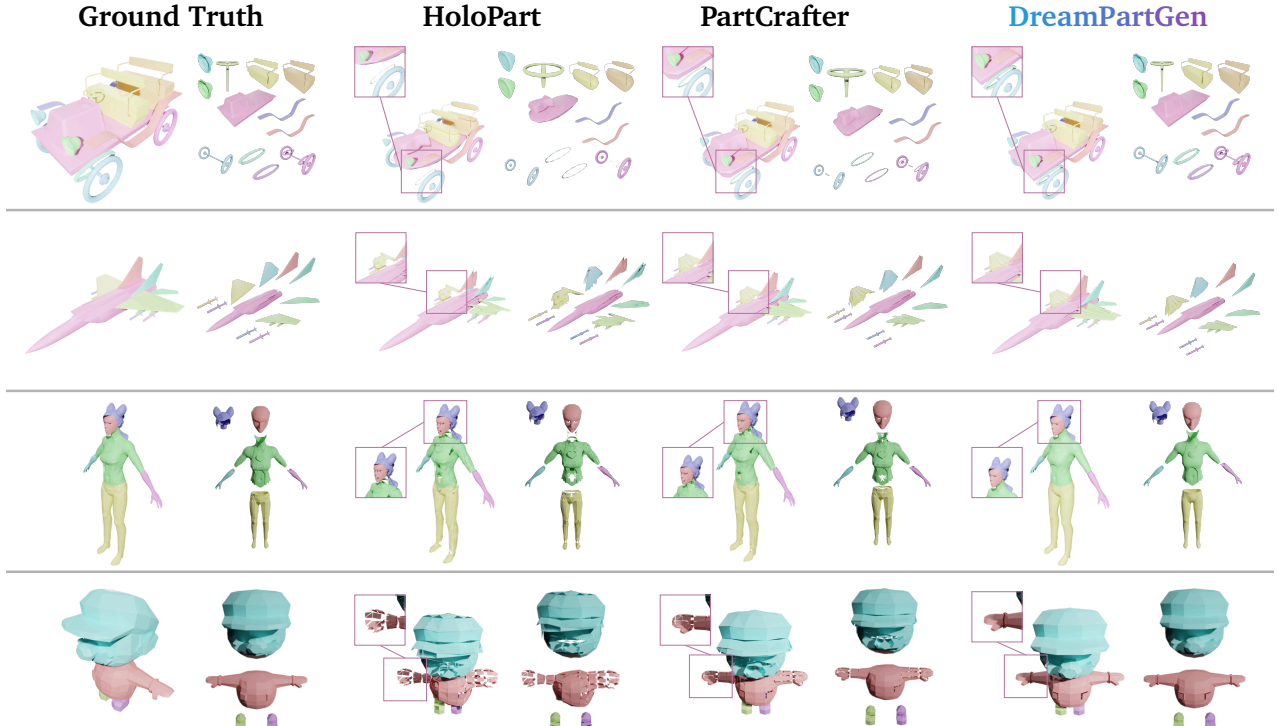


Figure 4: Qualitative comparison on part-level 3D generation. Across diverse object categories, **DreamPartGen** yields the most faithful decompositions, preserving clear part boundaries, correct topology, and consistent spatial alignment. Baselines frequently exhibit assembly failures such as missing or detached parts (e.g., wing/head), spatial drift of small components (e.g., wheels/mechanical parts floating off the chassis), and unstable attachments that create surface tearing or holes around high-contact regions (neck, torso, shoulders, limb joints).

performance: CD increases to 5.764 ($\uparrow 647.6\%$), EMD increases to 0.781 ($\uparrow 438.6\%$), IoU increases to 0.652 ($\uparrow 207.5\%$), and ULIP-T decreases to 0.089 ($\downarrow 43.7\%$), confirming the importance of jointly evolving part and semantic latents for stable generation. Finally, eliminating the part identifier module (**X Part Identifier**) also hurts disentanglement and semantics: IoU increases to 0.438 ($\uparrow 106.6\%$), CD/EMD increase to 1.709/0.277 ($\uparrow 121.7\%$ / $\uparrow 91.0\%$), and ULIP-T drops to 0.091 ($\downarrow 42.4\%$), showing it helps preserve identity-consistent structure.

Relational Semantic Latents (RSLs). We qualitatively analyze the roles of the local semantic \mathbf{S}^{loc} and global relational tokens \mathbf{S}^{glb} . For \mathbf{S}^{loc} , we compare against a conditioning-only baseline where text embeddings are injected only via timestep-wise cross-attention, without maintaining persistent semantic latents across denoising. As shown in Figure 5, conditioning-only yields coarser and less consistent

surface geometry, with weaker semantic coherence between parts, indicating that co-denoising with \mathbf{S}^{loc} is essential for high-fidelity part synthesis and semantic consistency. For \mathbf{S}^{glb} , we remove the persistent global relational tokens and their object-level synchronization while keeping part-level denoising unchanged. Without global relational guidance, parts remain plausible in isolation, but the assembled object exhibits increased inter-part misalignment, weaker structural coherence, and spatial drift (Figure 6), confirming that persistent global relational semantics are crucial for enforcing coherent object-level organization during denoising.

5.4. Downstream Applications

Text-to-3D Scene Generation. DreamPartGen enables a wide range of part-aware 3D applications, including text-to-3D scene generation. In this task, the goal is to generate a coherent multi-object scene



Figure 5: Ablation on the co-denoising process with local semantic tokens S^{loc} . The condition-only baseline ($-S^{\text{loc}}$) yields coarse geometry and weak semantic coherence between parts.



Figure 6: Ablation on the global relational tokens S^{glb} . The model exhibits part-level misalignment and spatial drift without S^{glb} .

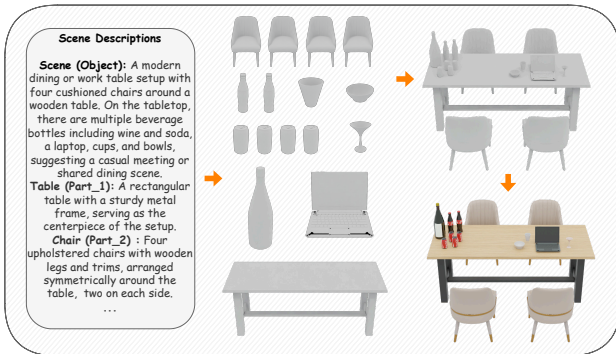


Figure 7: Mini-scene generation. Given a scene-level description, **DreamPartGen** can generate a complete, coherent 3D scene with physically plausible spatial layouts, capturing object geometry and fine-grained object- and part-level relations.

(a small scene) directly from a text prompt. During generation, each object is treated as a macro-part with aggregated DPLs, and a scene-level relational graph from canonicalized triplets (o_i, o_j, ρ) encodes spatial and functional relations. Objects are first generated independently and then jointly refined in a brief synchronization to produce the final, coherent scene. Additional details on the scene generation process can be found in the Appendix.

As shown in Figure 7, **DreamPartGen** can synthesize multi-object scenes that respect part structure, spatial constraints, and global coherence. **DreamPartGen**'s DPLs assign persistent, semantically meaningful slots for every part category, ensuring that the model



Figure 8: Part editing. From a source object (left), **DreamPartGen** can execute relational edit prompts to place accessories on top of or around the head, while preserving geometry and spatial consistency.

explicitly reasons over fine-grained sub-components (e.g., wooden chair legs) and part counts (e.g., four chairs). Additional examples are provided in Figure 1 (bottom right) and in the Appendix.

Text-to-3D Part Editing. To edit a specific part, we isolate its DPLs and freeze all others while keeping the global relational context fixed. We then apply localized re-denoising via partial DDIM inversion, optimizing only the target part's latents, followed by a brief synchronization step to restore coherence with the full object. As illustrated in Figure 8, **DreamPartGen** accurately executes relational part editing prompts, producing clean, high-fidelity edits with seamless part-to-part coherence. An additional editing example is shown in Figure 1 (top right). Details on the editing process, accompanied by more qualitative examples, can be found in the Appendix.

6. Conclusion

We introduce DreamPartGen, a part-aware text-to-3D generation framework that bridges geometric structure and semantic reasoning through collaborative part latent denoising. By coupling Duplex Part Latents (DPLs) with Relational Semantic Latents (RSLs), our method jointly models geometry, appearance, and inter-part relations, enabling coherent, interpretable, and controllable 3D synthesis. Beyond single-object generation, DreamPartGen enables a broad suite of part-centric applications, including relational part editing and compositional scene generation, highlighting the benefits of explicitly modeling 3D objects through structured, semantically grounded part latents. We hope this work motivates future research on controllable 3D generation and the role of structured part representations in more complex embodied or interactive settings.

References

- [1] Shuai Bai, Keqin Chen, Xuejing Liu, Jialin Wang, Wenbin Ge, Sibao Song, Kai Dang, Peng Wang, Shijie Wang, Jun Tang, et al. Qwen2. 5-vl technical report. *arXiv:2502.13923*, 2025.
- [2] Angel Chang, Will Monroe, Manolis Savva, Christopher Potts, and Christopher D Manning. Text to 3d scene generation with rich lexical grounding. In *Proceedings of the 53rd Annual Meeting of the Association for Computational Linguistics and the 7th International Joint Conference on Natural Language Processing (Volume 1: Long Papers)*, pages 53–62, 2015.
- [3] Angel X Chang, Thomas Funkhouser, Leonidas Guibas, Pat Hanrahan, Qixing Huang, Zimo Li, Silvio Savarese, Manolis Savva, Shuran Song, Hao Su, et al. Shapenet: An information-rich 3d model repository. *arXiv:1512.03012*, 2015.
- [4] Junsong Chen, Jincheng Yu, Chongjian Ge, Lewei Yao, Enze Xie, Yue Wu, Zhongdao Wang, James Kwok, Ping Luo, Huchuan Lu, et al. Pixart- α : Fast training of diffusion transformer for photorealistic text-to-image synthesis. *arXiv:2310.00426*, 2023.
- [5] Minghao Chen, Roman Shapovalov, Iro Laina, Tom Monnier, Jianyuan Wang, David Novotny, and Andrea Vedaldi. Partgen: Part-level 3d generation and reconstruction with multi-view diffusion models. In *IEEE Conference on Computer Vision and Pattern Recognition (CVPR)*, pages 5881–5892, 2025.
- [6] Rui Chen, Yongwei Chen, Ningxin Jiao, and Kui Jia. Fantasia3d: Disentangling geometry and appearance for high-quality text-to-3d content creation. In *International Conference on Computer Vision (ICCV)*, pages 22246–22256, 2023.
- [7] Yiwen Chen, Zhihao Li, Yikai Wang, Hu Zhang, Qin Li, Chi Zhang, and Guosheng Lin. Ultra3d: Efficient and high-fidelity 3d generation with part attention. *arXiv:2507.17745*, 2025.
- [8] Jasmine Collins, Shubham Goel, Kenan Deng, Achleshwar Luthra, Leon Xu, Erhan Gundogdu, Xi Zhang, Tomas F Yago Vicente, Thomas Dideriksen, Himanshu Arora, et al. Abo: Dataset and benchmarks for real-world 3d object understanding. In *IEEE Conference on Computer Vision and Pattern Recognition (CVPR)*, pages 21126–21136, 2022.
- [9] Matt Deitke, Dustin Schwenk, Jordi Salvador, Luca Weihs, Oscar Michel, Eli VanderBilt, Ludwig Schmidt, Kiana Ehsani, Aniruddha Kembhavi, and Ali Farhadi. Objaverse: A universe of annotated 3d objects. In *IEEE Conference on Computer Vision and Pattern Recognition (CVPR)*, pages 13142–13153, 2023.
- [10] Shaocong Dong, Lihe Ding, Xiao Chen, Yaokun Li, Yuxin Wang, Yucheng Wang, Qi Wang, Jaehyeok Kim, Chenjian Gao, Zhanpeng Huang, et al. From one to more: Contextual part latents for 3d generation. *arXiv:2507.08772*, 2025.
- [11] Zhirui Gao, Renjiao Yi, Yuhang Huang, Wei Chen, Chenyang Zhu, and Kai Xu. Partgs: Learning part-aware 3d representations by fusing 2d gaussians and superquadrics. *arXiv:2408.10789*, 2024.

-
- [12] Amir Hertz, Or Perel, Raja Giryes, Olga Sorkine-Hornung, and Daniel Cohen-Or. Spaghetti: Editing implicit shapes through part aware generation. *ACM Transactions on Graphics (TOG)*, 41(4):1–20, 2022.
- [13] Zhipeng Hu, Minda Zhao, Chaoyi Zhao, Xinyue Liang, Lincheng Li, Zeng Zhao, Changjie Fan, Xiaowei Zhou, and Xin Yu. Efficient-dreamer: High-fidelity and robust 3d creation via orthogonal-view diffusion priors. In *IEEE Conference on Computer Vision and Pattern Recognition (CVPR)*, pages 4949–4958, 2024.
- [14] Zehuan Huang, Yuan-Chen Guo, Xingqiao An, Yunhan Yang, Yangguang Li, Zi-Xin Zou, Ding Liang, Xihui Liu, Yan-Pei Cao, and Lu Sheng. Midi: Multi-instance diffusion for single image to 3d scene generation. In *IEEE Conference on Computer Vision and Pattern Recognition (CVPR)*, pages 23646–23657, 2025.
- [15] Diederik P Kingma and Max Welling. Auto-encoding variational bayes. *arXiv:1312.6114*, 2013.
- [16] Juil Koo, Seungwoo Yoo, Minh Hieu Nguyen, and Minhyuk Sung. Salad: Part-level latent diffusion for 3d shape generation and manipulation. In *International Conference on Computer Vision (ICCV)*, pages 14441–14451, 2023.
- [17] Hamid Laga, Michela Mortara, and Michela Spagnuolo. Geometry and context for semantic correspondences and functionality recognition in man-made 3d shapes. *ACM Transactions on Graphics (TOG)*, 32(5):1–16, 2013.
- [18] Songlin Li, Despoina Paschalidou, and Leonidas Guibas. Pasta: Controllable part-aware shape generation with autoregressive transformers. *arXiv:2407.13677*, 2024.
- [19] Weiyu Li, Rui Chen, Xuelin Chen, and Ping Tan. Sweetdreamer: Aligning geometric priors in 2d diffusion for consistent text-to-3d. *arXiv:2310.02596*, 2023.
- [20] Xinzhuo Li, Adheesh Juvekar, Jiaxun Zhang, Xingyou Liu, Muntasir Wahed, Kiet A Nguyen, Yifan Shen, Tianjiao Yu, and Ismini Lourentzou. Counterfactual segmentation reasoning: Diagnosing and mitigating pixel-grounding hallucination. *IEEE Conference on Computer Vision and Pattern Recognition (CVPR) Findings Track*, 2026.
- [21] Yixun Liang, Xin Yang, Jiantao Lin, Haodong Li, Xiaogang Xu, and Yingcong Chen. Lucid-dreamer: Towards high-fidelity text-to-3d generation via interval score matching. In *IEEE Conference on Computer Vision and Pattern Recognition (CVPR)*, pages 6517–6526, 2024.
- [22] Chen-Hsuan Lin, Jun Gao, Luming Tang, Towaki Takikawa, Xiaohui Zeng, Xun Huang, Karsten Kreis, Sanja Fidler, Ming-Yu Liu, and Tsung-Yi Lin. Magic3d: High-resolution text-to-3d content creation. In *IEEE Conference on Computer Vision and Pattern Recognition (CVPR)*, pages 300–309, 2023.
- [23] Yuchen Lin, Chenguo Lin, Panwang Pan, Honglei Yan, Yiqiang Feng, Yadong Mu, and Kateřina Fragkiadaki. Partcrafter: Structured 3d mesh generation via compositional latent diffusion transformers. *arXiv:2506.05573*, 2025.
- [24] Anran Liu, Cheng Lin, Yuan Liu, Xiaoxiao Long, Zhiyang Dou, Hao-Xiang Guo, Ping Luo, and Wenping Wang. Part123: part-aware 3d reconstruction from a single-view image. In *ACM SIGGRAPH 2024 Conference Papers*, pages 1–12, 2024.
- [25] Ruoshi Liu, Rundi Wu, Basile Van Hoorick, Pavel Tokmakov, Sergey Zakharov, and Carl Vondrick. Zero-1-to-3: Zero-shot one image to 3d object. In *International Conference on Computer Vision (ICCV)*, pages 9298–9309, 2023.
- [26] Yu Liu, Baoxiong Jia, Ruijie Lu, Junfeng Ni, Song-Chun Zhu, and Siyuan Huang. Building interactable replicas of complex articulated objects via gaussian splatting. In *International Conference on Learning Representations (ICLR)*, 2025.
- [27] Yuanzhe Liu, Jingyuan Zhu, Yuchen Mo, Gen Li, Xu Cao, Jin Jin, Yifan Shen, Zhengyuan
-

- Li, Tianjiao Yu, Wenzhen Yuan, et al. Palm: Progress-aware policy learning via affordance reasoning for long-horizon robotic manipulation. In *IEEE Conference on Computer Vision and Pattern Recognition (CVPR)*, 2026.
- [28] Ruijie Lu, Yu Liu, Jiayang Tang, Junfeng Ni, Yuxiang Wang, Diwen Wan, Gang Zeng, Yixin Chen, and Siyuan Huang. Dreamart: Generating interactable articulated objects from a single image. *arXiv:2507.05763*, 2025.
- [29] Shuqi Lu, Haowei Lin, Lin Yao, Zhifeng Gao, Xiaohong Ji, Yitao Liang, Linfeng Zhang, Guolin Ke, et al. Unified cross-scale 3d generation and understanding via autoregressive modeling. *arXiv:2503.16278*, 2025.
- [30] Niloy J Mitra, Michael Wand, Hao Zhang, Daniel Cohen-Or, Vladimir Kim, and Qi-Xing Huang. Structure-aware shape processing. In *ACM SIGGRAPH 2014 Courses*, pages 1–21. Association for Computing Machinery, 2014.
- [31] Kaichun Mo, Shilin Zhu, Angel X Chang, Li Yi, Subarna Tripathi, Leonidas J Guibas, and Hao Su. Partnet: A large-scale benchmark for fine-grained and hierarchical part-level 3d object understanding. In *IEEE Conference on Computer Vision and Pattern Recognition (CVPR)*, pages 909–918, 2019.
- [32] Kiet A Nguyen, Adheesh Juvekar, Tianjiao Yu, Muntasir Wahed, and Ismini Lourentzou. Calico: Part-focused semantic co-segmentation with large vision-language models. In *IEEE Conference on Computer Vision and Pattern Recognition (CVPR)*, pages 4550–4561, 2025.
- [33] Ben Poole, Ajay Jain, Jonathan T Barron, and Ben Mildenhall. Dreamfusion: Text-to-3d using 2d diffusion. *arXiv:2209.14988*, 2022.
- [34] Charles Ruizhongtai Qi, Li Yi, Hao Su, and Leonidas J Guibas. Pointnet++: Deep hierarchical feature learning on point sets in a metric space. *Advances in Neural Information Processing Systems (NeurIPS)*, 30, 2017.
- [35] Lingteng Qiu, Guanying Chen, Xiaodong Gu, Qi Zuo, Mutian Xu, Yushuang Wu, Weihao Yuan, Zilong Dong, Liefeng Bo, and Xiaoguang Han. Richdreamer: A generalizable normal-depth diffusion model for detail richness in text-to-3d. In *IEEE Conference on Computer Vision and Pattern Recognition (CVPR)*, pages 9914–9925, 2024.
- [36] Alec Radford, Jong Wook Kim, Chris Hallacy, Aditya Ramesh, Gabriel Goh, Sandhini Agarwal, Girish Sastry, Amanda Askell, Pamela Mishkin, Jack Clark, et al. Learning transferable visual models from natural language supervision. In *International Conference on Machine Learning (ICML)*, pages 8748–8763. PmLR, 2021.
- [37] Amit Raj, Srinivas Kaza, Ben Poole, Michael Niemeyer, Nataniel Ruiz, Ben Mildenhall, Shiran Zada, Kfir Aberman, Michael Rubinstein, Jonathan Barron, et al. Dreambooth3d: Subject-driven text-to-3d generation. In *International Conference on Computer Vision (ICCV)*, pages 2349–2359, 2023.
- [38] Licheng Shen, Saining Zhang, Honghan Li, Peilin Yang, Zihao Huang, Zongzheng Zhang, and Hao Zhao. Gaussianart: Unified modeling of geometry and motion for articulated objects. *arXiv:2508.14891*, 2025.
- [39] Yichun Shi, Peng Wang, Jianglong Ye, Mai Long, Kejie Li, and Xiao Yang. Mvdream: Multi-view diffusion for 3d generation. *arXiv:2308.16512*, 2023.
- [40] Jiayang Tang, Jiawei Ren, Hang Zhou, Ziwei Liu, and Gang Zeng. Dreamgaussian: Generative gaussian splatting for efficient 3d content creation. *arXiv:2309.16653*, 2023.
- [41] Jiayang Tang, Ruijie Lu, Zhaoshuo Li, Zekun Hao, Xuan Li, Fangyin Wei, Shuran Song, Gang Zeng, Ming-Yu Liu, and Tsung-Yi Lin. Efficient part-level 3d object generation via dual volume packing. *arXiv:2506.09980*, 2025.
- [42] Gemma Team, Morgane Riviere, Shreya Pathak, Pier Giuseppe Sessa, Cassidy Hardin, Surya

- Bhupatiraju, Léonard Hussenot, Thomas Mesnard, Bobak Shahriari, Alexandre Ramé, et al. Gemma 2: Improving open language models at a practical size. *arXiv:2408.00118*, 2024.
- [43] Muntasir Wahed, Kiet A Nguyen, Adheesh Sunil Juvekar, Xinzhuo Li, Xiaona Zhou, Vedant Shah, Tianjiao Yu, Pinar Yanardag, and Ismini Lourentzou. Prima: Multi-image vision-language models for reasoning segmentation. *arXiv:2412.15209*, 2024.
- [44] Zhengyi Wang, Cheng Lu, Yikai Wang, Fan Bao, Chongxuan Li, Hang Su, and Jun Zhu. Prolificdreamer: High-fidelity and diverse text-to-3d generation with variational score distillation. *Advances in Neural Information Processing Systems (NeurIPS)*, 36:8406–8441, 2023.
- [45] Jianfeng Xiang, Zelong Lv, Sicheng Xu, Yu Deng, Ruicheng Wang, Bowen Zhang, Dong Chen, Xin Tong, and Jiaolong Yang. Structured 3d latents for scalable and versatile 3d generation. In *IEEE Conference on Computer Vision and Pattern Recognition (CVPR)*, pages 21469–21480, 2025.
- [46] Le Xue, Mingfei Gao, Chen Xing, Roberto Martín-Martín, Jiajun Wu, Caiming Xiong, Ran Xu, Juan Carlos Niebles, and Silvio Savarese. Ulip: Learning a unified representation of language, images, and point clouds for 3d understanding. In *IEEE Conference on Computer Vision and Pattern Recognition (CVPR)*, pages 1179–1189, 2023.
- [47] Xinhao Yan, Jiachen Xu, Yang Li, Changfeng Ma, Yunhan Yang, Chunshi Wang, Zibo Zhao, Zeqiang Lai, Yunfei Zhao, Zhuo Chen, et al. X-part: high fidelity and structure coherent shape decomposition. *arXiv:2509.08643*, 2025.
- [48] Yunhan Yang, Yuan-Chen Guo, Yukun Huang, Zi-Xin Zou, Zhipeng Yu, Yangguang Li, Yan-Pei Cao, and Xihui Liu. Holopart: Generative 3d part amodal segmentation. *arXiv:2504.07943*, 2025.
- [49] Yunhan Yang, Yufan Zhou, Yuan-Chen Guo, Zi-Xin Zou, Yukun Huang, Ying-Tian Liu, Hao Xu, Ding Liang, Yan-Pei Cao, and Xihui Liu. Omnipart: Part-aware 3d generation with semantic decoupling and structural cohesion. *arXiv:2507.06165*, 2025.
- [50] Taoran Yi, Jiemin Fang, Junjie Wang, Guan-jun Wu, Lingxi Xie, Xiaopeng Zhang, Wenyu Liu, Qi Tian, and Xinggang Wang. Gaussian-dreamer: Fast generation from text to 3d gaussians by bridging 2d and 3d diffusion models. In *IEEE Conference on Computer Vision and Pattern Recognition (CVPR)*, pages 6796–6807, 2024.
- [51] Tianjiao Yu, Xinzhuo Li, Yifan Shen, Yuanzhe Liu, and Ismini Lourentzou. Core3d: Collaborative reasoning as a foundation for 3d intelligence. *arXiv:2512.12768*, 2025.
- [52] Tianjiao Yu, Vedant Shah, Muntasir Wahed, Kiet A Nguyen, Adheesh Juvekar, Tal August, and Ismini Lourentzou. Uncertainty in action: Confidence elicitation in embodied agents. *arXiv:2503.10628*, 2025.
- [53] Tianjiao Yu, Vedant Shah, Muntasir Wahed, Ying Shen, Kiet A Nguyen, and Ismini Lourentzou. Part²GS: Part-aware modeling of articulated objects using 3d gaussian splatting. In *IEEE Conference on Computer Vision and Pattern Recognition (CVPR)*, 2026.
- [54] Biao Zhang, Jiapeng Tang, Matthias Niessner, and Peter Wonka. 3dshape2vecset: A 3d shape representation for neural fields and generative diffusion models. *ACM Transactions on Graphics (TOG)*, 42(4):1–16, 2023.
- [55] Longwen Zhang, Ziyu Wang, Qixuan Zhang, Qiwei Qiu, Anqi Pang, Haoran Jiang, Wei Yang, Lan Xu, and Jingyi Yu. Clay: A controllable large-scale generative model for creating high-quality 3d assets. *ACM Transactions on Graphics (TOG)*, 43(4):1–20, 2024.
- [56] Xizhou Zhu, Yuntao Chen, Hao Tian, Chenxin Tao, Weijie Su, Chenyu Yang, Gao Huang, Bin Li, Lewei Lu, Xiaogang Wang, et al. Ghost in the minecraft: Generally capable agents for

open-world environments via large language models with text-based knowledge and memory. *arXiv:2305.17144*, 2023.

- [57] Zhe Zhu, Le Wan, Rui Xu, Yiheng Zhang, Honghua Chen, Zhiyang Dou, Cheng Lin, Yuan Liu, and Mingqiang Wei. Partsam: A scalable promptable part segmentation model trained on native 3d data. *arXiv:2509.21965*, 2025.

A. Implementation Details

We train **DreamPartGen** in two stages using the PartRel3D dataset introduced in Sec. 4. In the first stage, we optimize the part latent with semantic synchronization under the DPL-RSL interaction framework. The diffusion backbone adopts a Transformer-based DiT architecture with cross-attention layers that enable joint reasoning across modalities and parts. To enhance the part-level representation, we fine-tune the VAE using PartVerse [10] and PartNet [31]. In the second stage, we fine-tune the full model jointly, including both part-level and object-level synchronization, with persistent relational semantic latents providing structural conditions throughout denoising. The training objective employs an SNR-weighted curriculum that gradually shifts the emphasis from low-level denoising toward high-level semantic alignment, progressively strengthening relational and structural coherence across parts. We use AdamW with a learning rate of 1×10^{-4} , cosine decay, and gradient clipping at 1.0. All experiments are conducted on four NVIDIA L40 GPUs. To ensure fair comparison, all models are evaluated on the same test split of the selected datasets. Baseline methods are evaluated using their official publicly available implementations, following the protocols recommended in their repositories. All reported metrics are computed under the same evaluation pipeline.

B. PartRel3D Dataset

Canonicalization. When available, functional meta-data is directly converted into triplets; otherwise, relations are generated using a pretrained VLM [1] prompted with rendered views and part captions. Free-form relational phrases from captions or VLM outputs are normalized into $\mathcal{V}_{\text{spatial}}$ through a two-step process: (i) *Parsing*, where relational clauses are extracted from text (e.g., “the seat is positioned right above the legs”), and (ii) *Mapping*, where the phrase is aligned to the nearest canonical predicate (e.g., “positioned right above” \rightarrow above, “touches the body at the side” \rightarrow attached-to). Entities i and j are resolved to part indices using the Part-

Verse vocabulary or its synonyms. Ambiguities such as plural forms (“legs”) are resolved by mapping to all relevant slots, while singular references select a single part instance. Each triplet is interpreted as an assembly-level constraint that specifies how two parts are arranged. For example, (handle, body, attached-to) encodes a functional attachment, (wings, wings, symmetric-with) enforces bilateral symmetry, and (seat, legs, above) indicates the seat is supported by the legs.

Validation. To validate the generated functional and spatial relations in PartRel3D, we adopt a two-stage protocol. First, we perform *geometric checks* on spatial triplets using the ground-truth part geometry. Each part mesh is loaded into Open3D, and its axis-aligned bounding box is computed directly from vertex coordinates. Predicate-specific inequalities are then applied to filter inconsistent or contradictory relations; triplets violating these constraints are flagged and removed. Second, we conduct a *human audit* on the remaining triplets. In each run, we uniformly sample 200 triplets from the full dataset and manually verify their correctness using rendered multi-view images and part masks. We repeat this process 20 times to obtain a stable estimate of annotation quality across predicates and object types. Across all runs, spatial and functional triplets achieve an average correctness of 92% and 88%, respectively. During training, triplets are treated as *relational signals*: they are embedded as relational semantic latents and aggregated through attention, allowing the model to down-weight inconsistent or noisy triplets.

C. Additional Experiments

Qualitative Examples. Figure 9 illustrates the overall generation process, showing each stage of our framework from textual input to final 3D assembly. Given a textual input with optional image input, they are then enriched through articulated *functional* and *spatial triplets* (FT & ST). Leveraging these structured representations, the model synthesizes high-quality parts and semantically coherent objects. As shown in the last two columns, DreamPartGen successfully captures both individual parts and their global arrangement, enabling controllable and interpretable

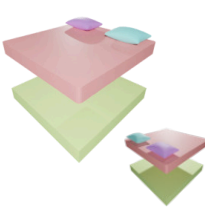
Image	Part Descriptions	FT & ST	Parts	Assembled Object
	<ol style="list-style-type: none"> 1. A bicycle wheel, which is part of the large bicycle depicted on the left. It features a black rim ... 2. A handlebar grip, which is part of a bicycle. The grip has sleek, aerodynamic shape ... 	FT:(wheel, frame, attach) FT:(seat, frame, support) FT:(gear, frame, attach) ... ST:(gear, frame, touching) ST:(gear, frame, right-of) ST:(seat, frame, above) ...		
	<ol style="list-style-type: none"> 1. A pillow likely made of soft fabric material with a slightly textured surface ... 2. A white rectangular base of a bed ... 3. A red mattress made of foam or similar material ... 	FT:(pillow_1, mattress, support) FT:(pillow_2, mattress, support) ... ST:(pillow_1, mattress, on-top-of) ...		
	<ol style="list-style-type: none"> 1. A skateboard deck without wheels ... 2. A skateboard truck with two wheels attached. It has visible bolts ... 3. Three skate board truck bolts with hexagonal head design ... 	FT:(wheel_1, board_1, attach) FT:(wheel_2, board_1, attach) ... ST:(wheel_1, board_1, below) ...		
	<ol style="list-style-type: none"> 1. A rugged off-road tire, which is part of a SUV ... 2. A long, horizontal metal bar with a silver finish ... 3. A yellow vehicle roof section , made of of durable material with a rugged appearance ... 	FT:(wheel_1, body, hinge) FT:(wheel_2, body, hinge) FT:(wheel_3, body, hinge) ... ST:(wheel_1, body, below) ST:(wheel_2, body, below) ST:(wheel_1, wheel_2, align-with) ...		
	<ol style="list-style-type: none"> 1. A candle holder with a textured, stone-like appearance ... 2. A candle characterized by its cylindrical shape and smooth feature ... 3. A circular beige base made of stone ... 	FT:(plate, candle_1, support) FT:(candle_1, flame, produce) ... ST:(plate, candle_1, below) ...		
	<ol style="list-style-type: none"> 1. A detailed view of an ear cup, which is part of an over-ear headphone ... 2. A sleek, black headband component of an over-ear headphone ... 3. An ear cup belong to an over-ear headphone ... 	FT:(left_ear_cup, headband, attach) FT:(right_ear_cup, headband, attach) ... ST:(left_ear_cup, right_ear_cup, symmetric-with) ...		

Figure 9: Qualitative Results. As illustrated, DreamPartGen enables high-quality part-aware 3D generation with no explicit structural guidance (e.g., bounding boxes).

Table 4: Perceptual evaluation on part-level 3D object generation. r-FID/r-KID refers to render-FID/render-KID computed from multi-view renderings. P-FID/P-KID computed in PointNet++ [34] feature space. Highlighted **best** and **second best**.

Method	Objaverse				ShapeNet				ABO				PartRel3D			
	r-FID	r-KID	P-FID	P-KID	r-FID	r-KID	P-FID	P-KID	r-FID	r-KID	P-FID	P-KID	r-FID	r-KID	P-FID	P-KID
Trellis	5.4873	0.0021	0.2314	0.0013	6.5142	0.0027	0.5159	0.0036	5.9238	0.0031	0.4476	0.0023	11.9827	0.0054	0.8453	0.0056
CLAY	5.2916	0.0019	0.2182	0.0012	6.3275	0.0024	0.4997	0.0034	5.8071	0.0029	0.4323	0.0021	11.7611	0.0052	0.8218	0.0054
HoloPart	4.9235	0.0018	0.2053	0.0011	5.8713	0.0022	0.4725	0.0032	5.3625	0.0024	0.4017	0.0019	10.9472	0.0048	0.7934	0.0050
PartCrafter	5.0147	0.0017	0.2129	0.0010	5.5387	0.0020	0.4513	0.0029	5.1184	0.0024	0.3829	0.0018	11.1359	0.0045	0.7517	0.0047
DreamPartGen	4.0579	0.0012	0.1684	0.0009	4.9736	0.0017	0.4128	0.0025	4.5632	0.0020	0.3495	0.0015	9.7836	0.0039	0.6921	0.0043

Table 5: Quantitative evaluation with different input settings. We evaluate DreamPartGen with different combinations of input information. Among single-source inputs, spatial triplets (ST) offer the greatest improvements, while functional triplets (FT) alone contribute weaker geometric constraints. Combining Text+Image+FT+ST yields the best overall performance across all metrics, highlighting the complementary benefits of language-grounded functional and spatial relations.

Condition	CD↓	EMD↓	r-FID↓	r-KID↓	P-FID↓	P-KID↓	CLIP(I-T)↑	ULIP-T↑
Image	1.272	0.174	8.573	0.0030	1.065	0.0020	0.235	0.155
Text	1.264	0.167	8.091	0.0026	1.210	0.0021	0.239	0.158
Functional Triplets (FT)	1.348	0.180	9.214	0.0031	1.324	0.0023	0.201	0.141
Spatial Triplets (ST)	1.321	0.179	8.932	0.0029	1.278	0.0022	0.214	0.147
Text+Image	0.771	0.145	6.753	0.0026	0.889	0.0015	0.238	0.158
Text+FT	0.821	0.150	7.032	0.0027	0.948	0.0016	0.241	0.164
Text+ST	0.298	0.112	6.842	0.0026	0.782	0.0016	0.245	0.169
Text+FT+ST	0.161	0.085	5.708	0.0018	0.701	0.0011	0.245	0.174
Text+Image+FT+ST	0.147	0.080	5.432	0.0018	0.725	0.0011	0.251	0.176

3D generation without explicit geometric supervision or bounding-box guidance.

Perceptual Evaluation. We report render-FID/KID and P-FID/P-KID separately in the Table 4. As shown, our model achieves the best perceptual performance across all four datasets, with HoloPart and PartCrafter alternating as the strongest baselines depending on the metric. These results mirror the trends observed in the geometric evaluations, further confirming the advantages of our relational-aware generative framework.

Condition-wise Analysis. Table 5 reports quantitative results under different conditioning setups. Among single-condition variants, spatial triplets (ST) deliver the largest improvement over text- or image-only baselines, achieving comparable or even better scores than the Text+Image setting. This confirms that language-grounded spatial relations provide strong geometric priors that guide assembly and alignment without requiring explicit 3D bounding-

box supervision. In contrast, functional triplets (FT) alone perform less effectively, as their high-level semantics (*e.g.*, *support*, *attach*, *hinge*) are linguistically abstract and do not directly constrain geometry. However, FT plays a complementary role by bridging the gap between textual intent and geometric structure. When combined with ST, it improves functional coherence across parts and stabilizes relational learning. Remarkably, the combined Text+FT+ST setting achieves performance that is competitive with, and in several metrics nearly matches, the full Text+Image+FT+ST configuration despite using no image input at all. The results show that our relational triplets can supply supervision, demonstrating that structured linguistic relationships (functional + spatial) can encode much of the geometric and compositional information typically learned from visual cues. Finally, adding image guidance (Text+Image+FT+ST) produces the strongest performance overall, confirming that visual evidence and relational reasoning are synergistic.

Table 6: Relation parsing robustness at inference. We compare three inference conditions for constructing relational triplets during test time: (1) with additional VLM (Qwen2.5-VL & ChatGPT-5), (2) oracle relations with ground-truth triplets, and (3) prompt-only conditioning. For the prompt-only row, we report the gap to the best-performing variant in each metric in parentheses. Highlighted **best** and **second-best**.

Method	r-FID↓	CD↓	ULIP-T↑	IoU↓
HoloPart	10.942	0.334	0.113	0.723
PartCrafter	11.134	0.312	0.109	0.717
DreamPartGen + Qwen2.5-VL	9.701	0.101	0.161	0.491
DreamPartGen + GPT-5	9.744	0.097	0.153	0.469
DreamPartGen + Oracle	9.684	0.101	0.161	0.471
DreamPartGen	9.783 (Δ 0.099)	0.099 (Δ 0.002)	0.153 (Δ 0.008)	0.474 (Δ 0.005)

Table 7: Quantitative evaluation on part-level 3D generation. We compare methods that explicitly generate part meshes on part-annotated datasets. **Best** and **second-best** results are highlighted.

Method	ShapeNet			PartRel3D		
	CD↓	EMD↓	F-Score↑	CD↓	EMD↓	F-Score↑
HoloPart	0.162	0.625	0.758	0.153	0.598	0.741
PartCrafter	0.141	0.603	0.732	0.137	0.612	0.756
DreamPartGen	0.088	0.451	0.863	0.081	0.438	0.772

Robustness to Relation Parsing. A key question is whether our model depends on a particular relational parser at inference time to supplement FT and ST, or whether the model has already internalized the relational structure knowledge. To study this, we evaluate three inference settings: (i) **VLM-parsed relations**, with two parser variants: the same VLM used for dataset construction (Qwen2.5-VL) and a stronger external parser (ChatGPT-5). (ii) **prompt-only conditioning** without explicit relation parsing, and (iii) **oracle relations** using ground-truth triplets. As shown in Table 6, prompt-only inference remains competitive, indicating that the model internalizes substantial part-level and assembly priors during training. The small gap between Qwen2.5-VL and ChatGPT-5 further suggests that the gains come from the RSL mechanism rather than parser-specific artifacts.

Part-Level Generation. Table 7 complements our object-level evaluation by measuring reconstruction fidelity on individual generated parts (CD, EMD, and F-score). We additionally report the F-score at threshold 0.005 by computing precision/recall between sampled points from the generated and ground-truth part surfaces. Across part-annotated

Table 8: Ablation on the number of local RSL tokens K_m . We vary the number of semantic controller tokens used for local relational-semantic guidance. Highlighted **best** and **second-best** results.

K_m	CD↓	EMD↓	IoU↓	CLIP(N-T)↑	CLIP(I-T)↑	ULIP-T↑
8	0.091	0.438	0.302	0.171	0.193	0.147
16	0.084	0.421	0.286	0.179	0.200	0.153
32	0.085	0.423	0.301	0.178	0.199	0.152
64	0.087	0.425	0.301	0.177	0.189	0.153

datasets, **DreamPartGen** consistently achieves the best per-part geometry quality, indicating that its gains are not only due to improved global assembly but also stronger generation of each component. In particular, the improvements in F-score show that **DreamPartGen** recovers more accurate part surfaces rather than merely reducing average distance metrics, confirming that the proposed DPL-RSL synchronization benefits fine-grained part geometry generation in addition to overall object coherence.

Number of Local RSL Tokens. RSLs act as semantic controllers, and their count K_m reflects the number of meaningful part-level attributes or relations. In PartRel3D, most objects contain roughly 10–30 such cues, so the token budget naturally remains small. We therefore evaluate $K_m \in \{8, 16, 32, 64\}$, a range that covers typical semantic density while keeping diffusion attention efficient. As shown in Table 8, performance stabilizes once $K_m \geq 16$, indicating that only a modest number of semantic tokens is needed for strong guidance. We set $K_m = 16$ as the default in all experiments.

Table 9: Robustness to rare parts and held-out relations. We evaluate in-distribution (ID) test data and two out-of-distribution (OOD) splits: OOD-parts (tail part labels) and OOD-rel (held-out relation predicates). We report absolute scores and the change relative to ID in parentheses (Δ).

Method	Split	r-FID↓	CD↓	ULIP-T↑	IoU↓
HoloPart	ID	10.942	0.334	0.113	0.723
	OOD-parts	12.318 (Δ 1.376)	0.392 (Δ 0.058)	0.101 (Δ 0.012)	0.781 (Δ 0.058)
	OOD-rel	12.701 (Δ 1.759)	0.408 (Δ 0.074)	0.098 (Δ 0.015)	0.797 (Δ 0.074)
PartCrafter	ID	11.134	0.312	0.109	0.717
	OOD-parts	12.206 (Δ 1.072)	0.358 (Δ 0.046)	0.097 (Δ 0.012)	0.759 (Δ 0.042)
	OOD-rel	12.583 (Δ 1.449)	0.371 (Δ 0.059)	0.094 (Δ 0.015)	0.771 (Δ 0.054)
DreamPartGen	ID	9.783	0.099	0.153	0.474
	OOD-parts	10.412 (Δ 0.629)	0.113 (Δ 0.014)	0.141 (Δ 0.012)	0.506 (Δ 0.032)
	OOD-rel	10.631 (Δ 0.848)	0.118 (Δ 0.019)	0.139 (Δ 0.014)	0.519 (Δ 0.045)

Generalization Beyond Clean Part Decompositions.

A key concern for part-based generators is reliance on clean, taxonomy-consistent part decompositions. To quantify robustness beyond the most common training configurations, we construct two out-of-distribution (OOD) evaluation splits that probe novel part and novel relation generalization. (i) **OOD-parts (rare-part split)**: we compute the training-set frequency of each part label (object-level occurrence) and define *rare* parts as those in the tail of this distribution, with a minimum-count filter (at least 2) to avoid noisy labels; the OOD-parts split includes all test objects that contain at least one rare part label. (ii) **OOD-rel (novel-relation split)**: we hold out a subset of relation predicates during training by removing all triplets whose predicate ρ belongs to a held-out set, and evaluate on test samples that include at least one held-out predicate. We report the same fidelity, alignment, and structure metrics as in the main evaluation (Render-FID, CD, ULIP-T, and IoU as a part-independence measure).

As shown in Table 9, all methods degrade under OOD shifts, but DreamPartGen exhibits smaller performance drops than prior part-based baselines: for example, under OOD-rel, PartCrafter increases from 11.134 to 12.583 in Render-FID (Δ 1.449), while DreamPartGen increases from 9.783 to 10.631 (Δ 0.848). Moreover, DreamPartGen maintains strong text-shape alignment under both splits (ULIP-T drops by only Δ 0.012-0.014), indicating that the learned relational priors generalize beyond the dominant

Table 10: Inference-time Comparison. We report per-sample inference latency. Methods are grouped by task type (object-level, part-level, or scene-level generation); timings should be interpreted within each row. **Best** time is highlighted.

Task	HoloPart	PartCrafter	TRELLIS	CLAY	MIDI	DreamPartGen
Object Gen.	-	-	95s	118s	-	45s
Part-level Gen.	21m	112s	-	-	-	109s
3D Scene Gen.	-	64s	-	-	102s	52s

training taxonomy and support coherent assembly even when parts or relations are less common.

Inference Efficiency. We compare per-sample inference latency across representative 3D generation methods in Table 10. Since these methods target different settings (object-level, part-level, and scene-level), we group comparisons by task type and interpret timings within each row. For DreamPartGen, we report the *prompt-only* setting to isolate the cost of the generative backbone; optional external VLM parsing is not required and is excluded from timing. The results show that DreamPartGen remains efficient despite its semantic synchronization design.

D. Applications

D.1. Mini-scene Generation

In this task, DreamPartGen generates a coherent multi-object arrangement (a small scene) directly from a text prompt that describes several semantically related objects and their spatial relations.

Table 11: Evaluation on 3D Object-Composed Scene Generation. We report results on **3D-Front** and an **Occluded** subset. We report CD↓, F-score↑, and IoU↓, together with inference runtime↓ per scene. Highlighted **best** and **second-best**.

3D Scene Generation	3D-Front			3D-Front (Occluded)			Run Time↓
	CD↓	F-Score↑	IoU↓	CD↓	F-Score↑	IoU↓	
MIDI [14]	0.1602	0.7931	0.0013	0.2591	0.6618	0.0020	80s
PartCrafter	0.1528	0.8085	0.0016	0.2387	0.7042	0.0022	42s
DreamPartGen	0.1495	0.8146	0.0012	0.2321	0.7128	0.0019	40s

During generation, we treat each object as a macro-part, represented by its aggregated DPLs (L_i^{3D}, L_i^{2D}) and a relational graph derived from scene-level captions. These scene graphs are constructed using the same canonicalization procedure, producing inter-object triplets (o_i, o_j, ρ) that describe spatial and functional relations. The resulting scene-level semantic tokens S^{scene} guide object placement through cross-object attention, ensuring spatial consistency while preserving each object’s internal structure. To synthesize a complete scene, objects are first sampled independently and then jointly refined by re-synchronizing their DPLs under S^{scene} . Quantitatively, Table 11 shows that DreamPartGen improves both geometric fidelity and compositional consistency over prior methods, achieving lower CD and higher F-score. Figure 10 further demonstrates that this process yields diverse, coherent mini-scenes.

D.2. Articulated Object Generation

To model articulation, we first construct paired configurations of the same object representing opposite canonical poses. Following [11, 53], we estimate per-part transformations $\mathcal{T}_i = (\mathbf{R}_i, \mathbf{t}_i)$ by aligning the corresponding parts across the two states. Each part is first identified through fixed part embeddings e_i , and the transformation parameters are derived via rigid motion fitting between the part’s geometry in the two poses. This yields a compact articulation field $\{\mathcal{T}_i\}_{i=1}^N$ describing how each part moves relative to its canonical configuration. Once transformations are obtained, we reconstruct articulated motion by applying \mathcal{T}_i to the canonical part meshes and reassembling the original objects. The resulting articulated objects maintain structural integrity across states and preserve semantic consistency through the persistent



Figure 10: Mini-scene Generation Results.

part embeddings. This setup allows us to visualize or simulate motion between poses without any re-optimization or diffusion-based retraining. As illustrated in Figure 11, our relationally grounded model naturally produces articulated 3D assets that preserve structural consistency across different motion states.

D.3. Part Editing

To edit a specific part, we isolate its DPLs using the part identifier and freeze all non-target slots, keeping the global relational context S^{glb} fixed. We then perform localized re-denoising via partial DDIM inversion: the object is inverted to an intermediate noise level τ , and only the target part’s 3D and 2D latents are optimized. Afterward, the updated DPLs are decoded and briefly re-synchronized with the rest of the object to ensure structural coherence. More results on part editing are available in Figure 12.

E. Broader Impacts

The ability to generate, compose, and edit 3D objects at the part level has broad implications across robotics, simulation, virtual content creation, and digital twin systems. DreamPartGen contributes to this space by offering a semantically grounded framework that produces structurally coherent, fine-grained 3D assets directly from language. This capability can enhance how embodied agents reason about objects, support richer interaction models in simulation, and accelerate the creation of editable assets for entertainment, industrial design, and education. In practical

settings, such compositional generation can reduce the cost and expertise barrier for producing accurate and customizable 3D models, benefiting designers, animators, and researchers who rely on physically meaningful structures.

At the same time, generative systems of this kind carry risks, including potential privacy concerns when reconstructing real-world objects, intellectual property considerations when producing stylized assets, and misuse in synthetic media pipelines. Although DreamPartGen is intended for research and educational use, we encourage responsible deployment practices that respect consent, attribution, and content integrity. Its modular and transparent design does not eliminate the need for careful governance. Deployment should still follow best practices around provenance, data consent, and domain-specific usage guidelines. Overall, we believe the benefits of controllable, semantically structured 3D generation outweigh the risks when accompanied by appropriate oversight and ethical use.



Figure 11: Part Articulation Results. Our relationally grounded **DreamPartGen** model naturally produces articulated 3D assets that preserve structural consistency across different motion states.



Figure 12: Additional Part Editing Results. **DreamPartGen** allows diverse yet consistent part-level 3D asset generation.